

Article

Natural and Chemically Modified Post-Mining Clays—Structural and Surface Properties and Preliminary Tests on Copper Sorption

Beata Jabłońska ^{1,*} , Mark Busch ², Andriy V. Kityk ³ and Patrick Huber ² 

¹ Faculty of Infrastructure and Environment, Czestochowa University of Technology, Brzeznicka St. 60a, 42-200 Czestochowa, Poland

² Institute of Materials Physics and Technology, Hamburg University of Technology (TUHH), Eißendorfer Straße 42, 21073 Hamburg, Germany; mark.busch@tuhh.de (M.B.); patrick.huber@tuhh.de (P.H.)

³ Faculty of Electrical Engineering, Czestochowa University of Technology, Armii Krajowej 17, 42-201 Czestochowa, Poland; andriy.kityk@univie.ac.at

* Correspondence: beata.jablonska@pcz.pl; Tel.: +48-34-32-50-917

Received: 5 October 2019; Accepted: 12 November 2019; Published: 14 November 2019



Abstract: The structural and surface properties of natural and modified Pliocene clays from lignite mining are investigated in the paper. Chemical modifications are made using hydrofluoric acid (HF), sulfuric acid (H₂SO₄), hydrochloric acid (HCl), nitric acid (HNO₃), sodium hydroxide (NaOH), and hydrogen peroxide (H₂O₂), at a concentration of 1 mol/dm³. Scanning electron microscopy is used to detect the morphology of the samples. Nitrogen adsorption isotherms were recorded to determine the specific surface area (SSA), mesoporosity, microporosity, and fractal dimensions. The raw clay has an SSA of 66 m²/g. The most promising changes in the structural properties are caused by modifications with HF or H₂SO₄ (e.g., the SSA increased by about 60%). In addition, the raw and modified clays are used in preliminary tests with Cu(II) sorption, which were performed in batch static method at initial Cu(II) concentrations of 25, 50, 80, 100, 200, 300, and 500 mg/dm³ in 1% aqueous suspensions of the clayey material. The maximum sorption of Cu(II) on the raw material was 15 mg/g. The structural changes after the modifications roughly reflect the capabilities of the adsorbents for Cu(II) adsorption. The modifications with HF and H₂SO₄ bring a similar improvement in Cu(II) adsorption, which is around 20–25% greater than for the raw material. The structural properties of investigated clays and their adsorptive capabilities indicate they could be used as low-cost adsorbents (e.g., for industrial water pretreatment).

Keywords: shale; waste rocks; coal gangue; porosity; specific surface area; fractal dimension; wastewater pretreatment

1. Introduction

Lignite extraction via surface mining results in the removal of accompanying minerals, which create an overburden of geological deposits above lignite. The overburden consists of loose sedimentary material (gravel and sand), plastic rocks (claystones and mudstone), and more compact rocks (sandstones, lake chalk, and others) [1]. There are no exact data for the overburden that arises each year due to surface mining, in particular due to lignite mining. In Poland, lignite mining requires the removal of 110–130 million m³ per year of overburden [1]. To roughly estimate the overburden removal in the world, the above number can be multiplied by the “lignite extraction in the world” (1342 × 10⁶ t) to “lignite extraction in Poland” (66 × 10⁶ t) ratio, to obtain around 2500 million m³ per year (2013). There are no specific data from individual mines on the amount of clays exploited during the extraction of lignite. It is estimated, however, that the quantities of mined overburden masses are

many times higher than the mass of lignite extracted. The clayey minerals covering the lignite beds create deposits with thickness ranging from a few meters to several dozen meters. For example, the average ratio of overburden to bed thickness ranges from 2.2:1 in Turów to 6.6:1 in Adamów [2].

Abundant resources of clays around the world and their low price contribute to their popularity. They are non-toxic, readily accessible, and easy to process and prepare. Depending on the quality parameters, clays from lignite mining are used mainly in the refractory industry in building ceramics, such as bricks, ceramic tiles, sanitary ware, and stoneware products. They are also used for the construction of waterproofing layers in landfills, for rock-sealing, and as insulation materials in water reservoirs [3,4]. Clays, including beidellite ones, have also been applied as natural sorbents in adsorption processes for water and wastewater treatment [5–11]. They often combine ion exchange and molecular sieve adsorptive properties, and are susceptible to a wide range of modifications to these properties [12]. The presence of active surface centers in clay minerals also makes them good catalysts for various reactions occurring in nature. They are used, for example, as catalysts for the removal of organic pollutants from water and in industrial processes [13,14]. They are active in cracking reactions [15], synthesis [16], polymerization [17], isomerization [18], and oxidation [19].

Sustainable and rational management of mineral resources requires searching for new methods for management of mining wastes. Therefore, although the focus of the research was directed to the structural and surface properties of post-mining waste rocks, the motivation was the possible use of beidellite clays from surface mining as inexpensive adsorbents of metal ions. The use of clays as low-cost adsorbents is in accordance with the directions for mining waste management indicated in directive 2006/21/EC on the management of waste from extractive industries [20]. There is also a noticeable trend of using natural materials in adsorption, including both waste rocks [21] as well as agricultural waste materials [22]. The clays as well as other materials are often modified thermally [23,24] or chemically [25–27] to enhance their adsorptive properties. As reported in [28], clay minerals are good adsorbents for metals, such as Cd(II), Cr(III), Cr(VI), Hg(II), Co(II), Cu(II), Zn(II), Pb(II), Ni(II), and Mn(II). Polluting substances containing metal ions are released into the environment with insufficiently treated industrial and municipal sewage, as well as with waters originating from runoff from agricultural areas [29] or metalliferous rocks [30]. Wastewater containing metal ions originates mainly in the processing of non-ferrous metals, in the textile and chemical industries, in electroplating, and in production of alloys, cables, and others [31]. Metal ions show strong toxic properties and pose a threat to living organisms. For example, an excess of copper in water is highly toxic to biological activity, which limits the self-cleaning processes [32]. Therefore, initial tests against Cu(II) sorption on the tested material were also performed. According to [28], the adsorption capacity for Cu(II) sorption on various clay minerals ranges from 2.35 mg/g on palygorskite to 54.07 mg/g on immobilized bentonite.

In the research, the naturally occurring as well as chemically modified beidellite clays from lignite mining are considered. The aim was to determine and enhance the structural and surface properties of Pliocene clays, as well as perform preliminary tests for Cu(II) sorption. Acidic, alkaline, and hydrogen peroxide modifications were tested. Although they produce adsorbents without highly ordered porous structures, they are simple and inexpensive, and can significantly increase the specific surface and porosity, leading to improvement in the adsorption of various contaminants. Acid activation consists of treating minerals with acid solutions. This results in the introduction of H_3O^+ ions into exchangeable positions, increased surface acidity and partial violation of the crystal structure, and changes in surface area and porosity. The aim is to obtain a partially dissolved material with increased surface area, porosity, and surface acidity [33]. During acid activation, the number of weakly acidic surface functional groups increases, while the number of groups with a stronger acidic character decreases. The dissolving of Al predominates over Si in acidic treatments. The materials produced are widely available, relatively inexpensive sources of protons, which are effective in many important reactions and processes for the industry [34]. Materials obtained in this way can be used to purify water, as well as wastewater from anthropogenic pollutants. Aluminates treated with acids are used as catalysts (e.g.,

in oil cracking). The main difference between acidic and alkaline activation of clay minerals is that in the first case, the process leads to degradation and amorphization of the original silicate structure, while in the second case, through the partial degradation stage, skeletal silicates with favorable sorption, ion-exchange, and catalytic properties can be formed. Bases were also used to obtain synthetic zeolites formed from kaolin and bentonite or from fly ash from coal combustion [35]. However, the course of these reactions is strongly dependent on factors such as the type and degree of ordering of the clayey matter, alkali concentration in the solution, time and temperature of activation, mixing intensity of the suspension, and the ratio between solid and liquid phases in the alkaline suspension.

2. Materials and Methods

2.1. Materials

The samples of clay rocks were taken from the Pliocene clayey sandy layers from an opencast lignite mine located in the central part of Poland. The lignite deposits, as well as accompanying sediments (clays, mud, and peat deposits), are associated with the tertiary formations of the Polish lowlands. The samples were acquired from a dump site where the beidellite clays are selectively stored as a waste mineral, which is used by the mine directly or after processing, but mostly for sale to external customers.

2.2. Sample Preparation

The samples were ground below a particle size of 100 μm and air dried. The analyses were done for the unmodified material as well as modified chemically by acidic, alkaline, and hydrogen peroxide activation to oxidize the organic components of the clays. The modifications were performed using the standard procedures described in [36–38]. Acidification of the samples was carried out with hydrofluoric, sulfuric, nitric, and hydrochloric acids. Alkaline activation was performed with sodium hydroxide. In the tests, 1 molar solutions of hydrofluoric acid (HF), H_2SO_4 , H_2NO_3 , HCl, NaOH, and H_2O_2 were used. Here, 30 g of raw clay was mixed with a 1 molar solution of the suitable chemical in a shaking water bath (357 type, Elpin-Plus s.c., Lubawa, Poland) at 70 $^\circ\text{C}$ for 6 h, after which the samples were allowed to stand for 14 h in solution. Finally, the precipitate was filtered off and washed several times with deionized water until reaching natural pH. The samples of the clays used in our investigations are marked as follows:

- S1—unmodified clay;
- S2—clay activated with HF;
- S3—clay activated with H_2O_2 ;
- S4—clay activated with H_2SO_4 ;
- S5—clay activated with HCl;
- S6—clay activated with HNO_3 ;
- S7—clay activated with NaOH.

2.3. Characterization of Material

The ash content (non-flammable constituents) was determined at 815 $^\circ\text{C}$ according to Polish standard PN-ISO 1171:2002P [39]. The chemical composition was determined via XRF (X-ray fluorescence) on a sequence spectrometer PW 1404 (Philips, Amsterdam, The Netherlands). Scanning electron microscopy (SEM) images were obtained on a Zeiss Supra 55 VP with 7.5 μm aperture and 2 nm resolution. The images were made for raw and modified samples in the form of powder of grain size below 100 μm . Nitrogen adsorption/desorption isotherms ($T = 77\text{ K}$) were measured, employing a commercial volumetric adsorption setup provided by Autosorb iQ (Quantachrome Instruments, relative uncertainty below 0.15%). The volume (v) of adsorbed nitrogen was measured as a function of the relative equilibrium pressure ($p/p_s = x$), where p is the equilibrium pressure, and p_s is the saturated

vapor pressure over the flat surface of the liquid. The relative pressure range was from around 10^{-5} to above 0.99. The nitrogen adsorption/desorption values were expressed in cm^3 @STP (at standard temperature and pressure) per gram of adsorbent. Prior to nitrogen adsorption, the clay samples were degassed at 105°C for several hours at a pressure of 10^{-4} mmHg.

The specific surface area was determined using standard BET (Brunauer-Emmett-Teller) technique (Equations (A1)–(A3) in Appendix A) with several linear forms of the BET Equation (A3). However, they all resulted in negative (i.e., non-physical) C values or poor matching with experimental data for some samples. Therefore, the modified BET equation (A4), which takes into account the finite number of adsorbate layers, n , was finally used. The value of n determined the best possible fit (i.e., to approach 1 for the determination coefficient (R^2)). The search interval was $1 \leq n \leq 5$.

The pore size distribution was calculated using the standard BJH (Barrett-Joyner-Halenda) method with the Kelvin equation. Calculations were performed using the standard Harkins–Jura statistical thickness of the adsorbate layer, as well as for the experimentally determined statistical thickness, whose values were tabulated in [40]. The details are given in Appendix A (Equations (A5)–(A7) and Figure A1).

The microporosity analysis was performed using the Dubinin–Radushkevich (DR) equation. Relative pressures up to 0.1 were considered. Calculations were also made using the Dubinin–Astakhov equation.

The microporosity was also evaluated via the t-plot method, with the statistical thickness of the adsorbate layer as mentioned above. The α_S analysis was performed using the Dunino given in [41] as the reference adsorbent. Its adsorption isotherm has a shape similar to the adsorption isotherms of the tested samples, and is characterized by $S_{\text{BET}} = 9.1 \text{ m}^2/\text{g}$ and $v(0.4) = 3.3087 \text{ cm}^3/\text{g}$ (STP).

The fractal dimension (D) is a measure of self-similarity of a geometrical object at various scales. For a surface, $2 \leq D < 3$, and the higher D the more folded and crimped the surface. Therefore, the fractal dimension is often used to characterize the surface of porous materials [42,43]. In this paper, it was calculated by applying the Kiselev equation and the method described in [44]. In accordance with this approach, the following equation is valid:

$$\ln \left[- \frac{\int_{v(x)}^{v_{\max}} \ln x dv(x)}{r_c^2(x)} \right] = \text{const} + D \ln \frac{(v_{\max} - v(x))^{\frac{1}{3}}}{r_c(x)}, \quad (1)$$

where $r_c(x)$ is the Kelvin radius corresponding to the relative pressure x . The value of D was calculated by fitting the experimental data with a straight line in the range of $0.4 \leq x \leq 0.99$. Equation (1) is similar to the equation resulting from the thermodynamic method [45], but the arrangement of the experimental points is almost rectilinear in the pressure range broader than in the thermodynamic method or the Frenkel–Halsey–Hill method.

2.4. Cu(II) Sorption

Sorption capacity for Cu(II) was determined for raw and chemically modified samples. Sorption tests were carried out using a synthetic solution of copper nitrate ($\text{Cu}(\text{NO}_3)_2 \cdot 3\text{H}_2\text{O}$) in batch static method. Water solutions of copper ions at initial concentrations of 25, 50, 80, 100, 200, 300, and $500 \text{ mg}/\text{dm}^3$ were added to 1% aqueous suspensions of clay. The pH of the solutions was 4 and was determined using a solution of $0.1 \text{ mol}/\text{dm}^3$ HCl or $0.1 \text{ mol}/\text{dm}^3$ NaOH. The flasks with prepared samples were shaken on a rotary shaker for 2 h at 20°C , after which they were placed in a dark room for 22 h. Then, the water from the conical flasks was decanted and centrifuged (MPW-2 type, MPW Med. Instruments, Warsaw, Poland) at 2500 rpm to remove the settling material from the solution. In the obtained eluates, the concentration of metal ions was analyzed using an inductively coupled plasma atomic emission spectrometer (ICP-AES). Three series of measurements were carried

out for each sample, and in the following considerations the average values are considered. The amount of metal absorbed (q) is calculated as follows:

$$q = \frac{C_i - C_e}{m} V \left[\frac{\text{mg}}{\text{g}} \right], \quad (2)$$

where C_i and C_e are the initial and equilibrium concentration of Cu(II), respectively, V is the volume of the solution, and m is the mass of the sediment. In mathematical description of Cu(II) adsorption, the Freundlich and Langmuir isotherms were used, along with Freundlich–Langmuir, two-site Langmuir, and several other more complicated isotherms [46]. However, apart from the Langmuir and Freundlich isotherms the estimates for errors of parameter values were usually larger than the parameter values. Therefore, only results for the Freundlich and Langmuir isotherms will be presented. The Freundlich isotherm is purely empirical and can be written as follows:

$$q = K_F C_e^n \quad \text{or} \quad \ln q = \ln K_F + n \ln C_e \quad (3)$$

where K_F and n are Freundlich isotherm parameters. The Langmuir isotherm is derived assuming a kinetic model of adsorption, and has the following form

$$q = \frac{Q K_L C_e}{1 + K_L C_e} \quad \text{or} \quad \frac{C_e}{q} = \frac{1}{Q K_L} + \frac{1}{Q} C_e \quad (4)$$

where Q (sorption capacity) and K_L (Langmuir constant) are Langmuir isotherm parameters. The values of parameters K_F , n , K_L , and Q were determined from the linear forms of the above equations.

3. Results and Discussion

3.1. Mineralogical and Chemical Composition

The rocks in the natural state have a light gray tint. In all samples, a high content of clay minerals was detected, ranging from 60% to 95%. The main clay minerals found in the mineral composition are smectites (beidelite), kaolinite, and calcite. In addition, quartz was found in small amounts in all samples, as well as trace amounts of siderite. The mentioned results for mineral composition are the average of three samples. The ash content is 91%, which corresponds to a loss on ignition (LOI) of about 9%. The chemical composition is presented in Table 1. It reflects the mineral composition. Large contents of SiO_2 and Al_2O_3 are related to the presence of beidellite, kaolinite, and quartz. A relatively low content of Na_2O results from lack of feldspars and micas in the examined clays.

Table 1. Chemical composition of the tested rocks.

Component	SiO_2	Al_2O_3	Fe_2O_3	CaO	MgO	Na_2O	K_2O	MnO	P_2O_5	TiO_2	SO_3	LOI
wt %	56.1	23.2	4.05	2.7	0.97	1.4	0.47	0.97	0.17	0.03	0.08	9.2

3.2. Nitrogen Adsorption and Desorption Isotherms

The nitrogen adsorption and desorption isotherms of the raw and chemically modified samples are presented in Figure 1. Hysteresis loops are visible on all of the isotherms. The adsorption and desorption branches join at a relative pressure of around 0.45. The hysteresis loops can be classified as H3/H4 (International Union of Pure and Applied Chemistry, IUPAC) or B/D (de Boer). H3 type is characteristic for loose aggregates of plate-like particles typical for some clays, and also in the case of pore networks containing macropores not completely filled with condensate. According to [47], H3-type loops indicate the presence of plaque-like mesopores with spaces between parallel plates. This seems to be confirmed in the subsequent section.

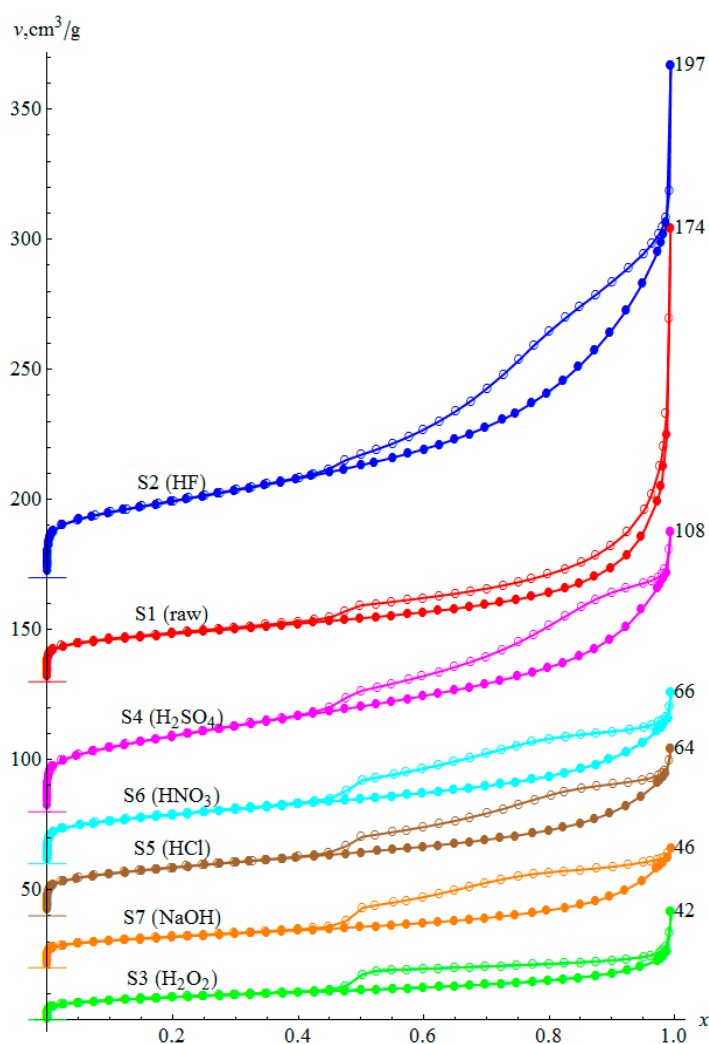


Figure 1. Isotherms of nitrogen adsorption and desorption in the samples tested. Consecutive isotherms are shifted vertically to avoid overlapping. The shifts are indicated by short horizontal lines on the vertical axis; the numbers on the right side of the graph show the adsorbate volume (STP) taken at a maximum relative pressure of about 0.995.

Classification of the isotherms themselves presents some difficulties. On the one hand, the presence of a hysteresis loop indicates type IV according to the IUPAC classification, but there is either no plateau characteristic for this type or it is difficult to observe (reduced to almost one point). On the other hand, the shape of the adsorption isotherms is best suited to type II, which in turn is characterized by a lack of hysteresis and no saturation at relative pressure near to 1; this is characteristic for nonporous and macroporous adsorbents [48]. Type II isotherms correspond to single- and multilayer physical adsorption on porous adsorbents. According to [49], the isotherms can be classified as pseudo-type II, describing delayed capillary condensation due to the small rigidity of the aggregate structure of the adsorbent.

Table 2 summarizes the pore volumes at the maximum pressure and the corresponding maximum pore sizes. These volumes cannot be compared directly because of the lack of a plateau on the isotherms, so Table 2 also shows volumes of pores filled at a relative pressure of 0.99, with a diameter of up to 190 nm (according to the Kelvin equation). These volumes range from 43 mm³/g for sample S3 to 227 mm³/g for S2. The pore volume in the raw sample is relatively large (165 mm³/g). The modification with HF increases this volume by approximately 37%, whereas the remaining modifications decrease it. The volume is slightly smaller in the sample treated with H₂SO₄, but in the samples modified with

HCl and HNO₃ the volume decreased about twice, and in the samples modified with NaOH and H₂O₂ to about 40% and 26% of the initial value respectively.

Table 2. Pore volume of the tested samples.

Parameter	S1 (Raw)	S2 (HF)	S3 (H ₂ O ₂)	S4 (H ₂ SO ₄)	S5 (HCl)	S6 (HNO ₃)	S7 (NaOH)
x_{\max}	0.997	0.994	0.995	0.994	0.994	0.995	0.996
d_{\max} , nm	295	319	375	300	317	377	463
V_{\max} , mm ³ /g ^a	270	305	65	167	99	102	72
$V(x = 0.99)$, mm ³ /g ^{a,b}	165	227	43	146	88	87	66

^a Evaluated as $V = kv$, where $k = 0.00154678$, v is volume at STP. ^b Volume of pores with diameter up to 190 nm (i.e., filled at a relative pressure of 0.99). Note: HF = hydrofluoric acid.

3.3. Morphology

SEM images of samples S1–S3 are presented in Figure 2. In all images there are visible plates, which confirm the above mentioned remark about H3-type loops. The SEM image for sample S2 is shown in Figure 2c. In comparison to the raw material (Figure 2a,b), the plates seem cleaner and more emphasized. As shown in the subsequent sections, sample S2 had one of the largest specific surface areas (SSA) out of the tested samples. Figure 2d shows the SEM image for sample S3, which turned out to have the lowest SSA. Indeed, the plates seem to be “dusty” and the spaces between them are filled and unavailable.

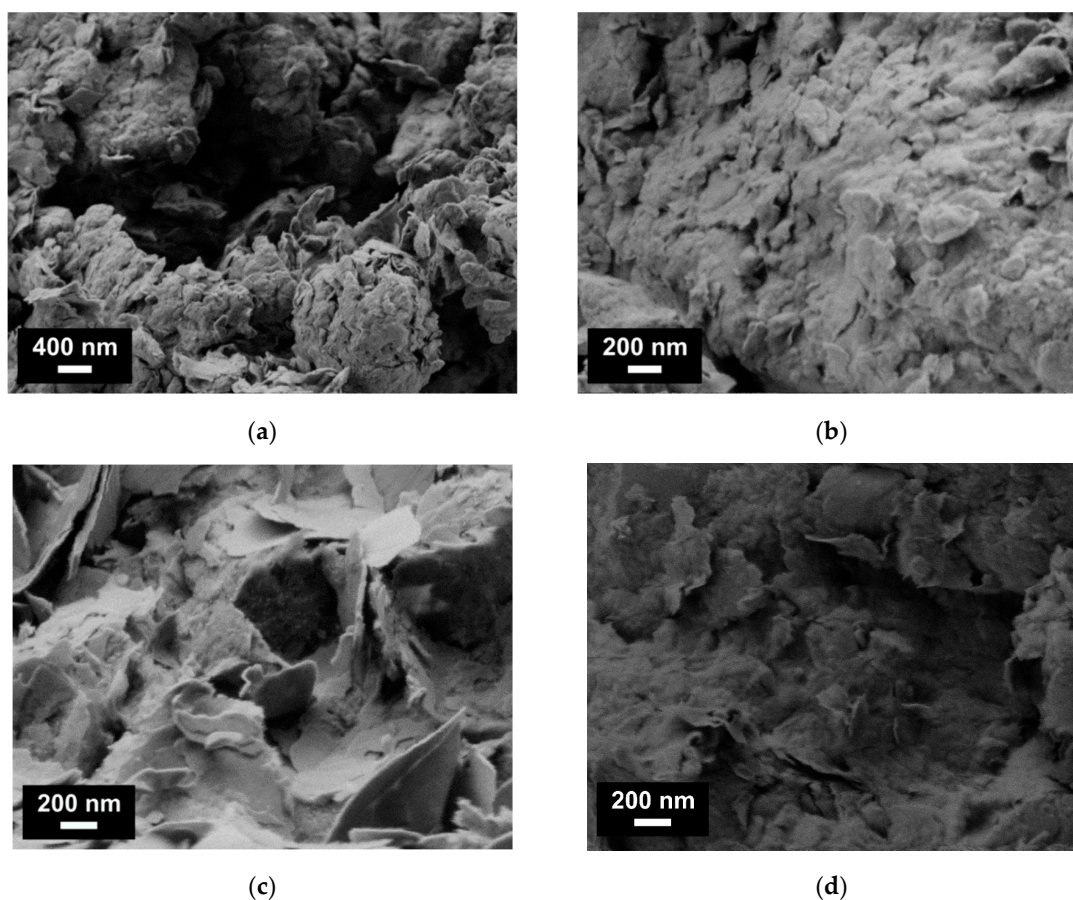


Figure 2. Scanning electron microscopy (SEM) images of tested samples: (a,b) raw sample (S1); (c) sample modified with HF (S2); (d) sample modified with H₂O₂ (S3).

3.4. Specific Surface Area

The parameters related to the SSA are shown in Table 3. The values of n fall in the range of 3–4.4 and the values of C range from 91 to 226, which means that point B (the knee) is well localized, and the interpretation of v_m as a monolayer volume is justified [48]. The determination coefficient (R^2) in all cases exceeds the value of 0.9999.

Table 3. Specific surface area (SSA) of the tested samples determined via modified BET method.

Parameter	S1 (Raw)	S2 (HF)	S3 (H ₂ O ₂)	S4 (H ₂ SO ₄)	S5 (HCl)	S6 (HNO ₃)	S7 (NaOH)
S_{BET} , m ² /g	66.1(1)	105.8(1)	32.0(1)	106.5(1)	67.0(1)	67.9(1)	42.8(1)
v_m , cm ³ /g (STP)	15.18(1)	24.30(1)	7.36(1)	24.48(1)	15.40(1)	15.61(1)	9.83(1)
n	3.1(1)	4.4(1)	3.0(1)	3.6(1)	3.1(1)	3.2(1)	3.1(1)
C	226(5)	122(3)	97(2)	91(2)	165(3)	173(4)	183(3)

The digit in the parentheses indicates the uncertainty of the preceding digit.

The values of the SSA range from 32 m²/g for sample S3 to 106.5 m²/g for sample S4. They can be described by relations $S4 \approx S2 > S6 \approx S5 \approx S1 > S7 > S3$. The raw rock is characterized by an SSA of ca. 66 m²/g. The activation with hydrofluoric or sulfuric acid increases the SSA up to approximately 106 m²/g (i.e., over 60%). The modification with nitric acid or hydrochloric acid practically has no influence on the SSA value. The sodium base modification, on the other hand, reduces the surface to about 43 m²/g, and the modification with hydrogen peroxide decreases the SSA more than twice (down to 32 m²/g). A similar SSA has been revealed, for example, in bentonite modified with HCl (84.6 m²/g) [50], as well as in a bentonite-based magnetic composite (94.81 m²/g) [51]. Bhattacharyya and Gupta [52] obtained an SSA of 19.8 m²/g for montmorillonite, which after modification with 0.25 mol/dm³ H₂SO₄ increased to 52.3 m²/g.

Acids may affect the structure and chemical composition of layered silicates in various ways. Changes in the structure of minerals depend on the type of layered silicate and acid treatment conditions (type of acid used, its concentration and temperature). The use of 1 mol/dm³ HF or H₂SO₄ was sufficient to affect the octahedral and partially tetrahedral layers, thus partially replacing Al²⁺, Mg²⁺, Fe³⁺, and other ions with hydronium ones. The activation with HF of low concentrations, in addition to partial degradation of the clay structure, causes substitution of OH[−] and network oxygen with F[−] ions [53]. This leads to an increase in the amount and power of active surface centers, in particular the acid centers of the Brønsted and Lewis type. Structural changes caused by fluorination increase the surface and porosity, mainly in the range of mesopores (Tables 3 and 4). This has been documented by studies on acidic properties of montmorillonite [54], as well as sepiolite [55].

Dissolution of silica tetrahedrons in the clay mineral structure is unlikely to occur at low acid concentrations (below ca. 0.1 mol/dm³), as they are relatively stable and their destruction occurs only at higher acid concentrations [56]. The use of more concentrated mineral acids can cause leaching of cations located in octahedral sublayers. Usually, these are Mg²⁺, Al²⁺, and Fe³⁺ cations. A part of them may form oxide aggregates in the solution under appropriate conditions. Octahedral layers, on the other hand, are much more susceptible to dissolving at low acid concentrations [57]. The structure of the tested clay minerals was significantly more resistant to 1 mol/dm³ HCl and HNO₃, which only revealed a slight increase in SSA.

Bases affect the structure of the silicates in various ways, too. In this case, the SSA of the sample modified with NaOH decreases. Hence, the base causes a passivation process, involving partial blockage of the pores. A similar effect was reported in [58]. Jozefaciuk and Bowanko [37] found strong elution of silica by NaOH from bentonite rocks. It is, therefore, likely that in the present case, NaOH elutes silica from the octahedral layers, which then completely or partially blocks the micropores and smaller mesopores. The absence of small mesopores is evident in Figure 3, depicting the pore size distribution.

The use of H_2O_2 to improve structural properties did not succeed, which was somewhat surprising, since activation with H_2O_2 usually increases the SSA [59]. However, it may also happen that the SSA was reduced [38]. This may be caused by several reasons affecting the effectiveness of H_2O_2 treatment, such as concentration, time of treatment, and presence of various catalysts, SiO_2 , and elements that build up in the mineral structure (e.g., iron) [60].

3.5. Mesoporosity

Although the BJH analysis is based on idealized pore geometries, it can deliver some information on mesoporosity. The analysis was performed for the statistical adsorbate thicknesses given in Appendix A. The most reliable results were assumed to be those for which the cumulative pore volumes were closest to relevant maximum values obtained from the adsorption isotherms. In each case, the best result was achieved for the thickness $t_{\text{Chj}}(x)$ (see Figure A1 in Appendix A). The size distribution of the pores is shown in Figure 3, whereas a comparison of the experimental results with the BJH analysis is presented in Table 4. The analysis with $t_{\text{Hj}}(x)$ gives similar results, but with clearly higher cumulative volume and area values.

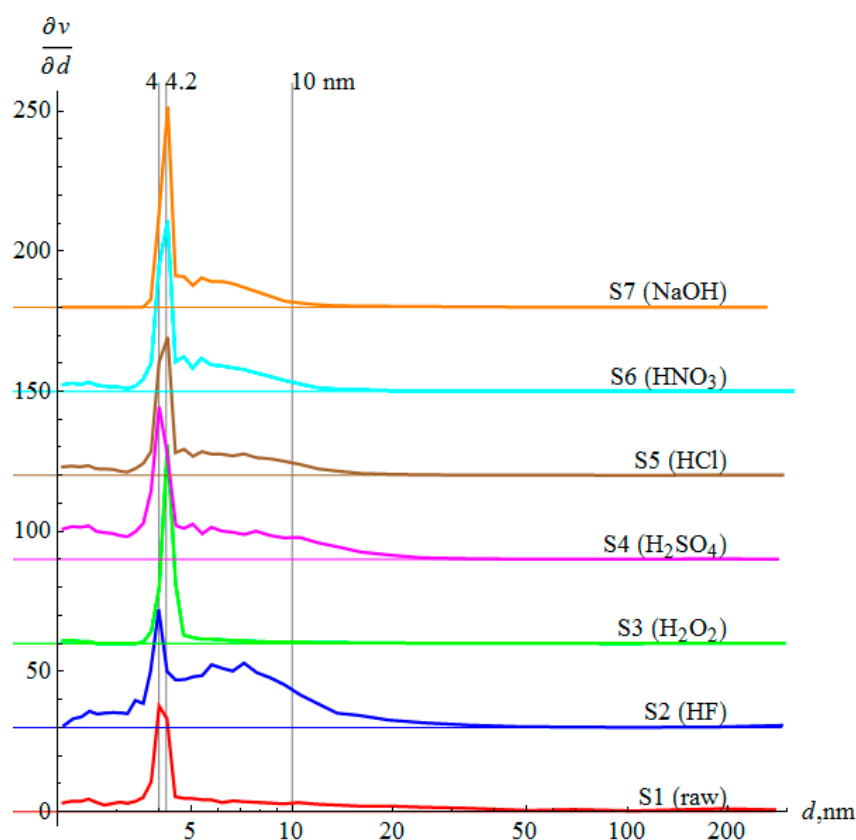


Figure 3. Pore size distributions of tested samples obtained using the BJH method with the statistical thickness of the adsorbate layer t_{Chj} ; to improve readability, the graphs are shifted vertically by a fixed value.

The dominant pore size is about 4.0 nm for samples S1, S2, and S4, and 4.2 nm for the remaining samples. However, the changes are very small and in the range of the uncertainty of the measurements and the analysis method. It is evident that neither HF nor H_2SO_4 increase the dominant pore size. The increase in SSA in this case results from the appearance of mesopores of size 2–15 nm (see Figure 3). In turn, HCl or HNO_3 increase the number of mesopores up to 10 nm in size. However, this does not cause a significant increase in the SSA. A small number of mesopores with a size up to 10 nm also appear in sample S7, but the mesopores of size below 4 nm seem to be almost eliminated, thus resulting

in a decrease in the SSA. A similar effect is apparent for sample S3, in which there are virtually no smaller or larger pores, so that only a portion of those dominant in the raw sample remains accessible for adsorption.

Table 4. Summary of BJH analysis results using statistical adsorbate thickness t_{Chj} ; for comparison, the pore volume obtained directly from the adsorption isotherm and BET surface area are also shown.

Parameter	S1 (Raw)	S2 (HF)	S3 (H ₂ O ₂)	S4 (H ₂ SO ₄)	S5 (HCl)	S6 (HNO ₃)	S7 (NaOH)
Pore size							
Dominant size, nm	4.0	4.0	4.2	4.0	4.2	4.2	4.2
Average size ^a , nm	15.2	9.9	7.1	5.5	5.5	5.5	6.2
Average size ^b , nm	16.3	11.5	8.1	6.3	5.9	6.0	6.7
Pore volume							
Total, mm ³ /g	269.5	305.1	64.5	166.9	99.3	101.8	71.6
Cumulative, mm ³ /g	269.6	320.1	68.3	180.6	105.0	108.2	78.9
macropores	177.9	113.1	28.3	31.2	18.6	21.5	8.6
mesopores	85.3	201.3	37.8	136.4	79.1	80.0	70.1
micropores ^c	6.4	5.7	2.2	13.1	7.3	6.7	0.2
Pore surface area							
BET, m ² /g	66.1	105.8	32.0	106.5	67.0	67.9	42.8
Cumulative, m ² /g	70.7	129.2	38.5	131.0	76.8	79.4	50.5
macropores	4.7	2.1	0.6	0.7	0.5	0.5	0.2
mesopores	46.8	107.8	31.2	92.8	54.6	58.7	49.5
micropores ^c	19.2	19.2	6.7	37.4	21.7	20.1	0.8

Note: ^a $4V_{cum}/S_{cum}$, ^b $4V_{max}/S_{BET}$, where V_{max} is the total pore volume. ^c Cumulative value minus meso- and macropore values.

The average pore size (assuming a cylindrical shape) was about 15 nm in the raw sample, whereas it decreased to 5.5–9.9 nm in the modified ones. The modifications, thus, led to either forming a number of pores with a diameter below 15 nm, or eliminating pores larger than 15 nm. This is consistent with earlier remarks.

In general, the cumulative volumes are usually larger than the measured ones. Likewise, the cumulative surface area is much larger than the one following from the BET analysis. This is due to the assumptions made in the BJH method concerning the shape of the pores as well as the assumed adsorbate thickness as a function of pressure. In spite of this, it is worth noting that the fraction of macropores evidently dominates in the raw sample (65% of the total pore volume), and the volume fraction of mesopores is about 31% of the total pore volume. After chemical treatment it considerably rises to above 50% of the total pore volume.

3.6. Microporosity

The results of microporosity analysis using the DR theory are shown in Table 5. The matching of the linear form of the DR equation to the experimental data was very good ($R^2 \geq 0.99$). The volume of micropores determined by this method ranges from about 12 mm³/g for sample S3 to about 37 mm³/g for sample S2. The volume of the micropores of the raw sample is about 25 mm³/g. The modifications with HF or H₂SO₄ result in an increase in micropore volume by about 50%. The other two acids (HCl and HNO₃) practically do not change the volume of the micropores. The use of NaOH significantly reduces this volume. The largest drop (by roughly 50%) was obtained with the use of H₂O₂. These results are consistent with the BET SSA values. The values of the exponent m according to the Dubinin–Astakhov theory were also calculated to get the best fit. The interval $2 \leq m \leq 5$ was considered. In each case, the best results were obtained for m at close to 2.

Table 5. Microporosity analysis.

Quantity	S1 (Raw)	S2 (HF)	S3 (H ₂ O ₂)	S4 (H ₂ SO ₄)	S5 (HCl)	S6 (HNO ₃)	S7 (NaOH)
DR theory							
V_0 , mm ³ /g	24.7(4)	36.9(8)	12.1(2)	36.5(7)	23.9(4)	25.0(4)	15.8(2)
t-plot							
V_{micro} , mm ³ /g	6.6(2)	3.9(2)	1.3(1)	2.3(1)	4.7(3)	4.8(3)	3.7(2)
S_{ext} , m ² /g	39.9(5)	75.8(5)	22.3(2)	78.1(3)	44.0(6)	44.6(6)	26.8(3)
S_{micro} , m ² /g	21.5(6)	27.4(6)	7.2(3)	23.6(4)	18.4(7)	19.3(7)	13.0(4)

The digits in the parentheses indicate the uncertainty of the preceding digits.

Table 5 also shows the results of t-plot analysis using the statistical layer thickness t_{CHJ} (the results using t_{HJ} were very similar). Although a linear fit of the experimental data in the range 1–1.5 monolayer thickness is very good (R^2 is close to 1), the volumes of micropores calculated using this method are much smaller than using the DR equation and range from 1.3 to 6.7 mm³/g. The relationships between samples are slightly different too—the largest volume of micropores was obtained in the raw sample. Modification with HCl or HNO₃ slightly reduces the content of micropores. Even smaller volumes of micropores are obtained for the samples modified with NaOH, as well as HF and H₂SO₄. The smallest micropore volume was for the sample treated with H₂O₂. The rather small volume of micropores for samples S2 and S4, deviating from the expected values greater than the raw sample, can be explained by the presence of relatively large micropores in these samples. They are not yet fully filled at the monolayer formation stage, and the assumptions of the t-plot method are not true in such a case.

The external surface area fulfills the relations analogous to the total SSA determined by the BET method. The surface area of micropores, understood as the difference between the BET surface and the external surface, is 21.5 m²/g in the raw sample. The modification with HF or H₂SO₄ increases this surface, whereas other modifications reduce it. The largest (almost a three-fold) drop is observed in a sample modified with H₂O₂.

The results of the α_S analysis of the examined samples are presented in Figure 4. Two α_S ranges were considered: 0.5–0.9 and 2–5. The tables included in the drawings show the available surface area and the volume of already filled pores at particular stages. The slope of the straight line in the first interval, approximately corresponding to the formation of a monolayer, is proportional to the surface area. These values agree with the results obtained using the BET method. The intersection of this line with the vertical axis indicates the volume of pores occupied in the previous condensation stage. For S2 and S4, the lines intersect slightly below zero, so it is assumed that the intersection is at zero in these cases.

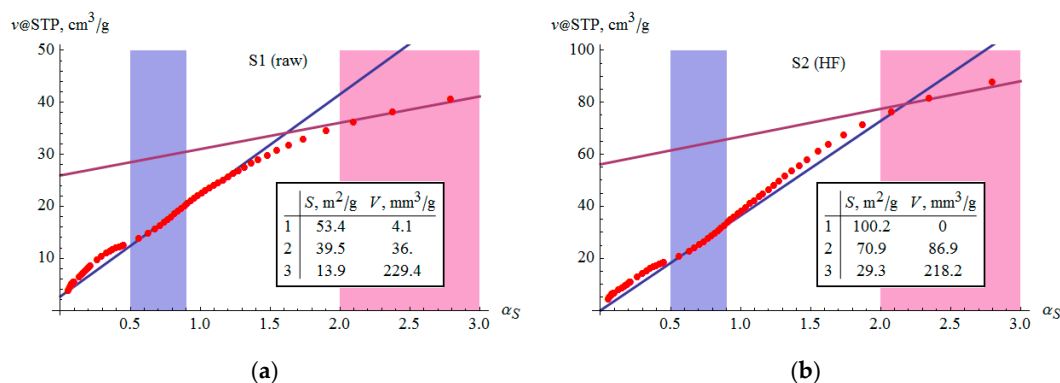


Figure 4. Cont.

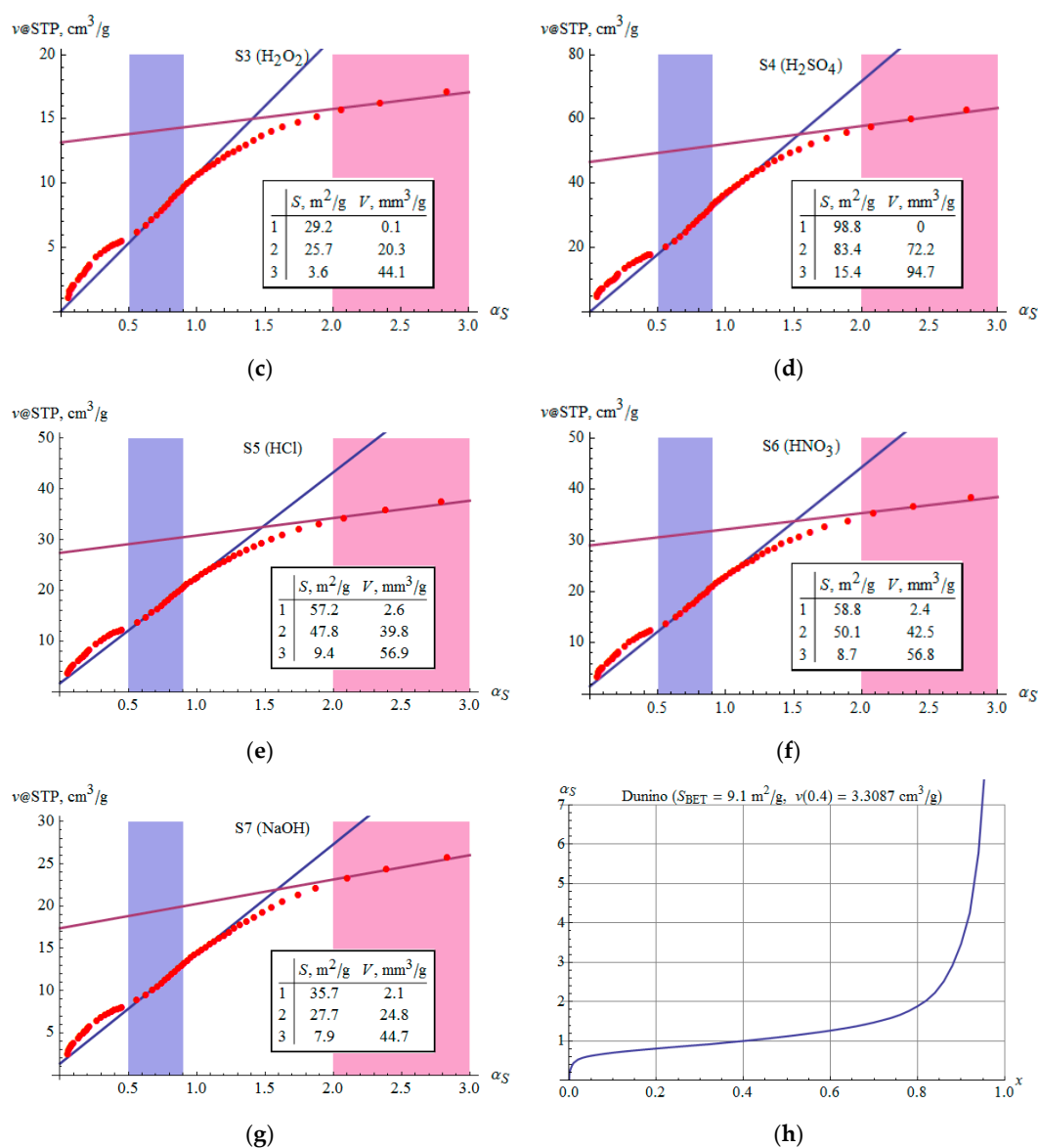


Figure 4. Results of the α_S analysis of the examined samples: (a–g) correspond to samples S1–S7 (red dots—measurement, blue line—fit for region shaded in blue, magenta line—fit for region in magenta); (h) the Dunino reference adsorbent data.

The presented α_S graphs do not contain the characteristic c-swing associated with capillary condensation (except for sample S2, in which a slight c-swing is noticeable). This is because capillary condensation takes place at high relative pressures in the samples under consideration, which is characteristic for pseudo-second-type isotherms. However, all samples are characterized by a distinct f-swing, indicating the presence of micropores.

3.7. Fractal Dimension

The results of the fractal dimension are shown in Table 6. The relative pressure range was 0.4–0.99. Matching the data to a straight line is very good ($R^2 > 0.99$). The smallest fractal dimension is observed in the raw sample (2.49–2.55). Acid modifications cause an increase in the dimension to about 2.72–2.93. The treatment with NaOH results in a similar increase in the fractal dimension. The smallest increase in the fractal dimension is recorded for the H₂O₂ modified sample (2.58–2.61). It is worth noting that

the fractal dimension was also calculated using the thermodynamic and Frenkel–Halsey–Hill methods, but in both cases the range of data linearity was much smaller.

Table 6. Fractal dimension of tested samples.

Quantity	S1 (raw)	S2 (HF)	S3 (H ₂ O ₂)	S4 (H ₂ SO ₄)	S5 (HCl)	S6 (HNO ₃)	S7 (NaOH)
D_{ads}	2.49(1)	2.72(1)	2.61(2)	2.75(1)	2.74(1)	2.76(1)	2.75(1)
D_{des}	2.55(1)	2.84(3)	2.58(6)	2.89(3)	2.92(4)	2.93(4)	2.98(3)

The digits in the parentheses indicate the uncertainty of the preceding digits.

3.8. Cu(II) Sorption

Changes in the Cu(II) concentration in the solution as a result of sorption processes are presented in Figure 5. The amount of sorbed Cu(II) ions increased in the series H₂O₂ < NaOH < raw ≈ HCl ≈ HNO₃ < H₂SO₄ < HF. The raw sample was characterized by a maximum sorption (obtained at the initial concentration of 500 mg/dm³) equal to about 15 mg/g. Similar values were obtained for samples modified with HCl and HNO₃. The samples modified with HF and H₂SO₄ proved to be the best sorbents of copper ions (maximum sorption capacity of about 19 mg/g and 18 mg/g, respectively). The adsorbents showing the weakest Cu(II) sorption are samples modified with NaOH and H₂O₂. They adsorbed 13 mg/g and 12 mg/g of Cu(II), respectively, at the maximum initial concentration of metal in the solution. The cation exchange capacity (CEC) of the studied clays is between 31.68 and 57.41 cmol₍₊₎/kg [61]. Comparing the maximum amount of copper ions retained with their CEC, it was found that Cu(II) ions in all samples tested were bound below the CEC value. All values of sorption capacity obtained in the experiment are lower than for activated carbons and also some biosorbents, such as pomegranate peels, for which the maximum sorption capacity values were 43.47 mg/g and 30.12 mg/g, respectively [62,63]. On the other hand, they are similar to those obtained for kaolinite and montmorillonite and their acid-activated forms, for which the Langmuir monolayer capacity was 4.3–28.0 mg/g [64] and much higher than for unmodified bentonite (8.33 mg/g) [65].

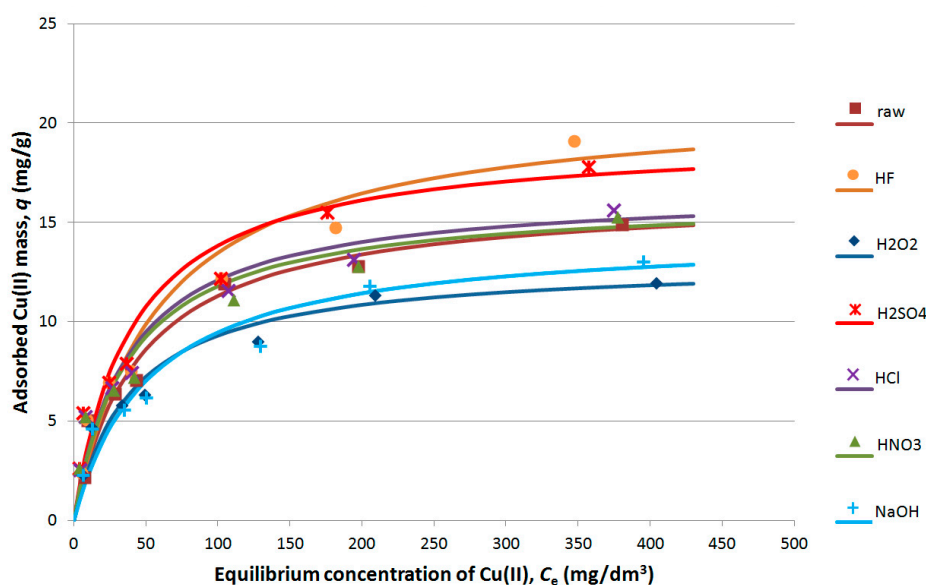


Figure 5. Langmuir isotherms (lines) and experimental values (markers) of Cu(II) adsorption on the tested samples.

Based on the obtained results, the parameters of Freundlich and Langmuir isotherms were determined (Table 7), obtaining in all cases a better fit for the Langmuir model (R^2 from 0.976 to 0.993), although in the case of Freundlich isotherms it was also acceptable (R^2 from 0.871 to 0.948).

For this reason, only the Langmuir isotherms are shown in Figure 5. The highest ability for Cu(II) retention by samples S2 and S4 is confirmed by the Langmuir maximum adsorptive capacity, Q , which is 21 ± 1 mg/g and 19 ± 1 mg/g, respectively. This means an improvement in the adsorption capacity by 29% and 18%, respectively. The higher K_L value for the S4 sample means that the adsorbent saturation occurred at lower values of copper ion concentration than in the case of S2.

Table 7. Parameters of Freundlich and Langmuir isotherms for Cu(II) sorption on the tested clays.

Parameter	S1 (Raw)	S2 (HF)	S3 (H ₂ O ₂)	S4 (H ₂ SO ₄)	S5 (HCl)	S6 (HNO ₃)	S7 (NaOH)
Freundlich isotherm							
K_F , mg/g dm ³ⁿ /mg ⁿ	1.4(4)	1.4(3)	1.4(3)	1.9(3)	1.8(3)	1.9(3)	1.3(2)
n	0.43(7)	0.46(5)	0.38(5)	0.40(4)	0.38(5)	0.36(4)	0.41(4)
R^2	0.871	0.943	0.926	0.943	0.933	0.948	0.945
Langmuir isotherm							
Q , mg/g	16.4(7)	21(1)	13.0(5)	19(1)	16.7(7)	16.2(8)	14.4(9)
K_L , dm ³ /mg	0.022(4)	0.017(4)	0.025(4)	0.025(5)	0.027(5)	0.027(6)	0.019(4)
R^2	0.992	0.976	0.993	0.987	0.990	0.987	0.983

Note: R^2 —determination coefficient; the digits in the parentheses indicate the uncertainty of the preceding digits.

Good estimation of the experimental data by the Langmuir isotherm confirms that the binding of copper ions by the clay is limited to the monomolecular layer covering the entire surface of the adsorbent. Cu(II) ions may, thus, be bound by chemisorption (specific sorption) to form stable ionic or covalent bonds between metal ions and the sorbent surface [66]. Strong binding of copper ions is very beneficial due to their immobilization, low susceptibility to release, and reduction of reactivity.

The sorption of copper ions on the tested materials decreases with an increase in the initial concentration of Cu(II) (Figure 6). The percentage of sorption is considerable and ranges from 19% to 86% for the initial concentrations tested. The percentage of sorption for raw material is from 56% to 80% at lower initial Cu(II) concentrations. At an initial concentration of 500 mg/dm³, it is 23% for the natural sample and about 30% for the acid-activated HF and H₂SO₄ (S2 and S4); however, for S3 and S7 samples activated with base and hydrogen peroxide, the percentage of sorption is about 20%. Samples S3 and S7 adsorbed the smallest amounts of Cu(II), most likely as a result of the passivation process, which is reflected in SSA and porosity changes (Tables 3–5).

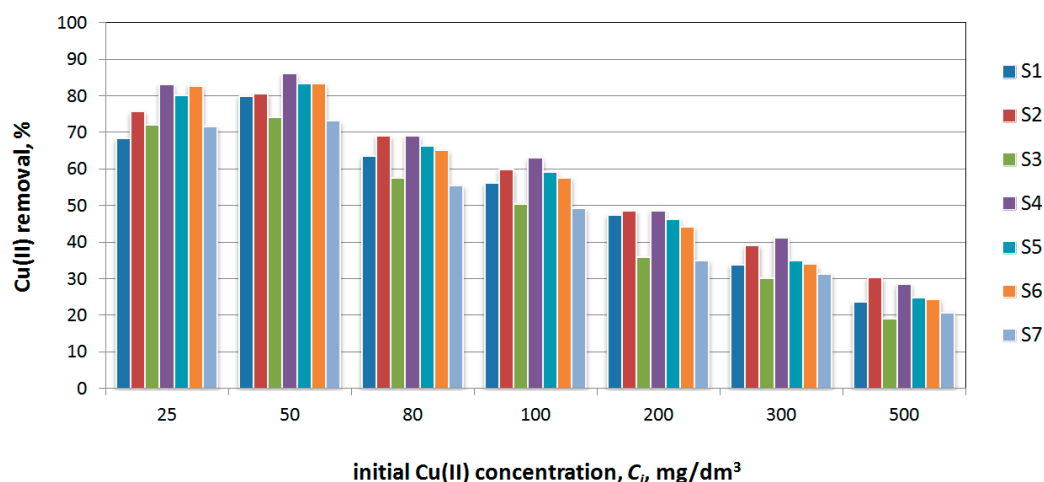


Figure 6. Cu(II) removal efficiency on the tested adsorbents.

3.9. Industrial Wastewater Pretreatment

The results presented in the above sections indicate that the considered post-mining rocks could be used as low cost adsorbents for industrial wastewater pretreatment. The idea of the process is presented in Figure 7. First, the rocks are prepared for metal ion adsorption. After grinding them to a suitable grain size, the material is placed in the adsorption column. Alternatively, it can be modified by a $1 \text{ mol/dm}^3 \text{ H}_2\text{SO}_4$ or $1 \text{ mol/dm}^3 \text{ HF}$ before placement in the column, but this stage is optional and may only be required to enhance the adsorption process. The raw industrial wastewater is directed into the settling tank for preliminary sedimentation and pH correction. The decanted wastewater is then transferred to the column for metal ion adsorption. The pretreated wastewater can then be directed for another treatment stage, depending on the degree of contamination and the required degree of purification. To enhance the adsorption process and avoid unnecessary downtime, two or more columns can be used in a cycle, so that when one column is working the other is being prepared for use by cleaning and filling with another portion of adsorbent. The used adsorbent can be directed for utilization, or alternatively it can be washed and reused in another cycle of the adsorption process.

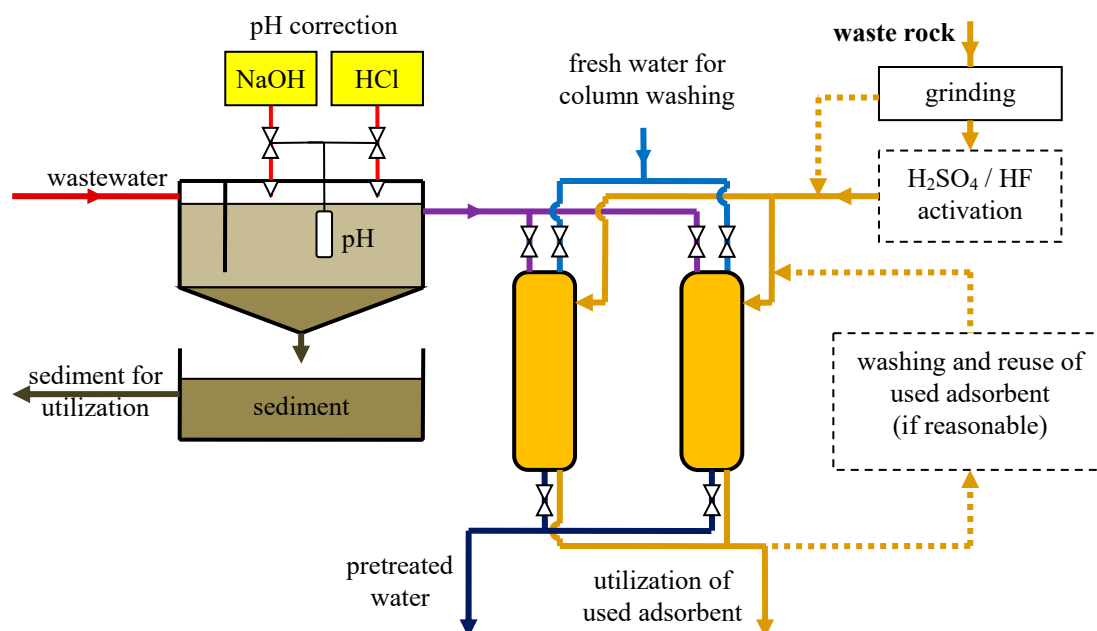


Figure 7. Use of post-mining waste rocks in industrial wastewater pretreatment.

4. Conclusions

Based on the above results, the following conclusions can be formulated:

- Raw clays under testing have an SSA of approximately $66 \text{ m}^2/\text{g}$; modifications with $1 \text{ mol/dm}^3 \text{ HF}$ or H_2SO_4 increase the SSA over 60%; modifications with $1 \text{ mol/dm}^3 \text{ HCl}$ or HNO_3 practically do not change the SSA; treatment with $1 \text{ mol/dm}^3 \text{ NaOH}$ or H_2O_2 results in a significant decrease in SSA. The SSA of the tested samples can be described by relations: $\text{H}_2\text{SO}_4 \approx \text{HF} > \text{HNO}_3 \approx \text{HCl} \approx \text{raw} > \text{NaO} > \text{H}_2\text{O}_2$.
- Adsorption isotherms (pseudo-second type with H3 hysteresis loop) indicate the presence of non-rigid aggregates, which is typical for some clays.
- Chemical treatment changes the pore size distribution—acids produce small and medium mesopores, NaOH removes small mesopores, and H_2O_2 comprises the majority of mesopores.
- The volume of micropores according to DR theory corresponds to relations analogous to the SSA. The presence of micropores is also confirmed by α_s analysis.

- The fractal dimension of the raw sample is 2.49–2.55. After chemical treatment, it increases to 2.61–2.98.
- Cu(II) sorption results reflect the structural and surface changes in the samples. The highest sorption capacity is obtained for modifications with HF or H₂SO₄.
- The investigated clays may be considered as prospective inexpensive adsorbents. Two aspects of cleaner production are obtained, in lignite extraction as well as in ion metal removal from specific industrial wastewater. For such a purpose, HF and H₂SO₄ produce the most favorable changes—they result in a significant increase in SSA, the formation of small and medium mesopores, as well as micropores (according to the DR theory). This shows a reflection in tests of Cu(II) sorption.

Author Contributions: Conceptualization, B.J.; methodology, B.J.; software, B.J.; validation, M.B., A.V.K., and P.H.; formal analysis, A.V.K. and P.H.; investigation, B.J. and M.B.; resources, B.J.; data curation, B.J. and M.B.; writing—original draft preparation, B.J.; writing—review and editing, A.V.K., M.B., and P.H.; visualization, B.J. and M.B.; supervision, B.J.

Funding: The APC was funded by Czestochowa University of Technology.

Acknowledgments: This work was financially supported by the Faculty of Infrastructure and Environment at the Czestochowa University of Technology under BS-PB-400-301/19. SEM images courtesy of Jens Timmermann, Hamburg University of Technology.

Conflicts of Interest: The authors declare no conflict of interest.

Appendix A

The specific surface area was determined as follows

$$S = \frac{V_m}{V_{\text{mol}}} \omega_m N, \quad (\text{A1})$$

where V_m is the monolayer volume of the liquid adsorbate (cm³/g), V_{mol} is the molar volume of liquid adsorbate (cm³/mol), ω_m is the effective cross-sectional area per adsorbate molecule (m²), N is the Avogadro number. The value of V_m is expressed as kv_m , where $k = 0.00154678$ is a conversion factor, and v_m is the monolayer volume (cm³@STP/g). Using the standard data for nitrogen at the temperature $T = 77$ K ($\omega_m = 0.162$ nm², $V_{\text{mol}} = 34.67$ cm³/g), one obtains

$$S = 4.35 \frac{\text{m}^2/\text{g}}{\text{cm}^3\text{@STP/g}} \times v_m. \quad (\text{A2})$$

The value of v_m was determined via BET equation, applying its several commonly used forms in the relative pressure range 0.05–0.35. The BET equation has the following form:

$$v = \frac{v_m C x}{(1-x)(1+(C-1)x)}, \quad (\text{A3})$$

where v is the volume of adsorbent at relative pressure x and C is a positive constant. Values of v_m and C can be calculated from adsorption isotherms. Several linear forms of Equation (A3) were used. However, they all resulted in negative (i.e., non-physical) C values, or poor matching with experimental data for some samples. Therefore, we decided to use a modified BET equation, which takes into account the finite number of adsorbate layers, n , in the following linear form:

$$\frac{x[1-x^n - nx^n(1-x)]}{v(1-x)^2} = \frac{1}{v_m C} + \frac{1}{v_m} \frac{x(1-x^n)}{1-x}. \quad (\text{A4})$$

The value of n is not necessarily an integer. In this paper, n was determined to get the best possible fit (i.e., to approach 1 for the determination coefficient (R^2)). The search interval was $1 \leq n \leq 5$.

The pore size distribution was calculated using the standard BJH method with the Kelvin equation

$$r_c(x) = -\frac{2\sigma V_{\text{mol}}}{RT \ln x}, \quad (\text{A5})$$

which gives the meniscus radius (Kelvin radius) corresponding to the relative pressure x . Here, σ is the surface tension of the adsorbate, R is the gas constant, and T is the temperature. The pore radius (r) is evaluated as

$$r(x) = r_c(x) + t(x) = t(x) - \frac{0.9542}{\ln x} [\text{nm}], \quad (\text{A6})$$

where t is the statistical thickness of the adsorbate on the pore wall at relative pressure x . The second form refers to liquid nitrogen. Calculations were performed using the standard Harkins–Jura statistical thickness of the adsorbate layer

$$t_{\text{HJ}} = 0.1 \sqrt{\frac{13.99}{0.034 - \log x}} \text{ nm} \quad (\text{A7})$$

as well as for the experimentally determined statistical thickness $t_{\text{CHJ}}(x)$, whose values were tabulated in [40]. The thicknesses are presented in Figure A1.

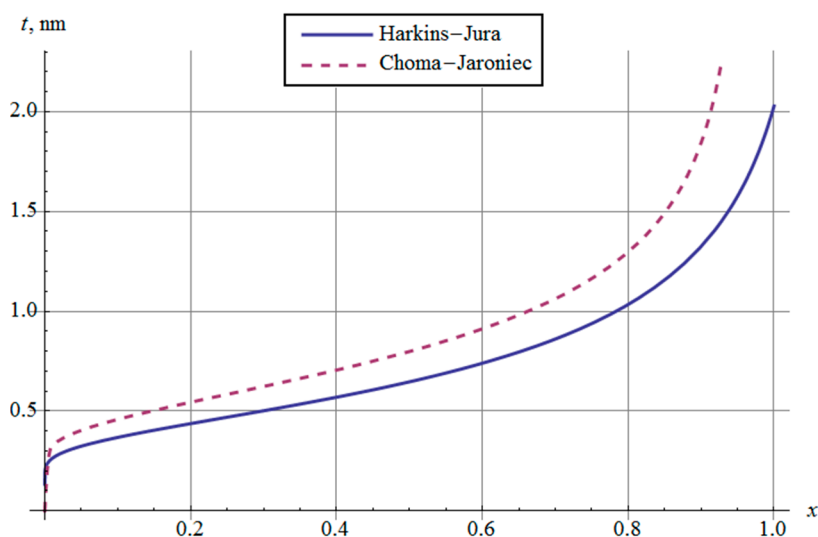


Figure A1. Statistical adsorbate thickness according to Harkins–Jura and Choma–Jaroniec considered in BJH analysis.

The microporosity analysis was performed using the DR equation, expressed as follows:

$$\ln V = \ln V_0 - \left(\frac{RT}{E} \ln \frac{1}{x} \right)^2, \quad (\text{A8})$$

where V is the volume of micropores filled at the relative pressure x , V_0 is the total volume of micropores, E is the characteristic energy depending on fluid–solid system. Relative pressures up to 0.1 were considered. The Dubinin–Astakhov equation permits the exponent of $m \geq 2$ instead of 2.

References

1. Ratajczak, T.; Bahranowski, K.; Górniak, K.; Szydłak, T.; Wyszomirski, P. Kopaliny towarzyszące. In *Eksploatacja Selektywna Węgla Brunatnego I Kopalini Towarzyszących Wraz Z Uwarunkowaniami Techniczno-Ekonomicznymi I Korzyściami Ekologicznymi*; Stryszewski, M., Ed.; Wydawnictwo CPPGSMiE PAN: Cracow, Poland, 1995; pp. 45–74.
2. Ratajczak, T.; Hycnar, E.; Jończyk, W. Złoże węgla brunatnego Bełchatów a problemy eksploatacji surowców skalnych i ceramicznych. *Biul. PIG* **2008**, *429*, 157–161.
3. Adamczyk, K.; Jończyk, M.W.; Skórzak, A. Kopaliny towarzyszące eksploatacji złoża węgla brunatnego Bełchatów—Historia dokumentowania i zagospodarowania. *Kalendarium. Górnictwo Odkryw.* **2012**, *1–2*, 25–41.
4. Galos, K.; Kot-Niewiadomska, A. Możliwości i perspektywy stosowania surowców ilastych z kopalni węgla brunatnego. *Górnictwo Odkryw.* **2012**, *1–2*, 15–19.
5. Kyzioł-Komosińska, J.; Rosik-Dulewska, C.; Pająk, M.; Czupioł, J.; Dzieniszewska, A.; Krzyżewska, I. Sorption of acid Green 16 from aqueous solution onto low-moor great and smectite clay co-occurring in lignite of Belchatow Mine Field. *Annu. Set Environ. Prot.* **2015**, *17*, 165–187.
6. Jabłońska, B.; Siedlecka, E. Removing heavy metals from wastewaters with use of shales accompanying the coal beds. *J. Environ. Manag.* **2015**, *155*, 58–66. [[CrossRef](#)] [[PubMed](#)]
7. Jabłońska, B. Sorption of phenol on rock components occurring in mine drainage water sediments. *Int. J. Miner. Process.* **2012**, *104–105*, 71–79. [[CrossRef](#)]
8. Zhou, L.; Zhou, H.; Hu, Y.; Yan, S.; Yang, J. Adsorption removal of cationic dyes from aqueous solutions using ceramic adsorbents prepared from industrial waste coal gangue. *J. Environ. Manag.* **2019**, *234*, 245–252. [[CrossRef](#)]
9. Ngulube, T.; Gumbo, J.R.; Masindi, V.; Maity, A. An update on synthetic dyes adsorption onto clay based minerals: A state-of-art review. *J. Environ. Manag.* **2017**, *191*, 35–57. [[CrossRef](#)]
10. Pernyeszi, T.; Farkas, R.; Kovács, J. Methylene Blue Adsorption Study on Microcline Particles in the Function of Particle Size Range and Temperature. *Minerals* **2019**, *9*, 555. [[CrossRef](#)]
11. Cuevas, J.; Dirocie, N.; Yunta, F.; Delgado, C.G.; Santamaría, D.E.G.; Ruiz, A.I.; Fernández, R.; Eymar, E. Evaluation of the Sorption Potential of Mineral Materials Using Tetracycline as a Model Pollutant. *Minerals* **2019**, *9*, 453. [[CrossRef](#)]
12. Sprynskyy, M. *Heterogeniczność Strukturalna Oraz Właściwości Adsorpcyjne Adsorbentów Naturalnych*; Wydawnictwo Naukowe UMK: Toruń, Poland, 2012.
13. Ding, Z.; Klopogge, J.T.; Frost, R.L. Porous Clays and Pillared Clays-Based Catalysts. Part 2: A Review of the Catalytic and Molecular Sieve Applications. *J. Porous Mater.* **2001**, *8*, 273–293. [[CrossRef](#)]
14. Akri, M.; Achak, O.; Granger, P.; Wang, S.; Batiot-Dupeyrat, C.; Chafik, T. Autothermal reforming of model purified biogas using an extruded monolith: A new catalyst based on nickel incorporated illite clay promoted with MgO. *J. Clean. Prod.* **2018**, *171*, 377–389. [[CrossRef](#)]
15. Kooli, F.; Liu, Y.; Hbaieb, K.; Al-Faze, R. Characterization and catalytic properties of porous clay heterostructures from zirconium intercalated clay and its pillared derivatives. *Microporous Mesoporous Mater.* **2016**, *226*, 482–492. [[CrossRef](#)]
16. Del Mar Orta, M.; Martín, J.; Medina-Carrasco, S.; Santos, J.L.; Aparicio, I.; Alonso, E. Novel synthetic clays for the adsorption of surfactants from aqueous media. *J. Environ. Manag.* **2018**, *206*, 357–363. [[CrossRef](#)] [[PubMed](#)]
17. Saleh, T.A.; Tuzen, M.; Sar, A. Polyamide magnetic palygorskite for the simultaneous removal of Hg(II) and methyl mercury; with factorial design analysis. *J. Environ. Manag.* **2018**, *211*, 323–333. [[CrossRef](#)] [[PubMed](#)]
18. Jackson, T.A. Preferential polymerization and adsorption of L-optical isomers of amino acids relative to D-optical isomers on kaolinite templates. *Chem. Geol.* **1971**, *7*, 295–306. [[CrossRef](#)]
19. Banković, P.; Milutinović-Nikolić, A.; Mojović, Z.; Jović-Jovičić, N.; Perović, M.; Spasojević, V.; Jovanović, D. Synthesis and characterization of bentonites rich in beidellite with incorporated Al or Al-Fe oxide pillars. *Microporous Mesoporous Mater.* **2013**, *165*, 247–256. [[CrossRef](#)]
20. Directive 2006/21/EC of the European Parliament and of the Council of 15 March 2006 on the Management of Waste from Extractive Industries and Amending Directive 2004/35/EC. Available online: <https://eur-lex.europa.eu/legal-content/EN/ALL/?uri=CELEX%3A32006L0021> (accessed on 1 October 2019).

21. Helios-Rybicka, E.; Wójcik, R. Competitive sorption/desorption of Zn, Cd, Pb, Ni, Cu, and Cr by clay-bearing mining wastes. *Appl. Clay Sci.* **2012**, *65–66*, 6–13. [[CrossRef](#)]
22. Osman, A.I.; Ahmed, A.T.; Johnston, C.R.; Rooney, D.W. Physicochemical characterization of Miscanthus and its application in heavy metals removal from wastewaters. *Environ. Prog. Sustain. Energy* **2017**, *27*, 1058–1067. [[CrossRef](#)]
23. Jabłońska, B.; Kityk, A.V.; Busch, M.; Huber, P. The structural and surface properties of natural and modified coal gangue. *J. Environ. Manag.* **2017**, *190*, 80–90. [[CrossRef](#)]
24. Lu, P.; Chen, T.; Liu, H.; Li, P.; Peng, S.; Yang, Y. Green Preparation of Nanoporous Pyrrhotite by Thermal Treatment of Pyrite as an Effective Hg(II) Adsorbent: Performance and Mechanism. *Minerals* **2019**, *9*, 74. [[CrossRef](#)]
25. Deihimi, N.; Irannajad, M.; Rezai, B. Characterization studies of red mud modification processes as adsorbent for enhancing ferricyanide removal. *J. Environ. Manag.* **2018**, *206*, 266–275. [[CrossRef](#)] [[PubMed](#)]
26. Leal, P.V.B.; Magriotis, Z.M.; de Sales, P.F.; Papini, R.M.; de Magalhães Viana, P.R. Effect of the acid treatment conditions of kaolinite on etheramine adsorption: A comparative analysis using chemometric tools. *J. Environ. Manag.* **2017**, *197*, 393–403. [[CrossRef](#)] [[PubMed](#)]
27. Vollprecht, D.; Frühauf, S.; Stocker, K.; Ellersdorfer, M. Ammonium Sorption from Landfill Leachates Using Natural and Modified Zeolites: Pre-Tests for a Novel Application of the Ion Exchanger Loop Stripping Process. *Minerals* **2019**, *9*, 471. [[CrossRef](#)]
28. Uddin, M.K. A review on the adsorption of heavy metals by clay minerals, with special focus on the past decade. *Chem. Eng. J.* **2017**, *308*, 438–462. [[CrossRef](#)]
29. Gliniak, M.; Sobczyk, W. Zawartość metali toksycznych w glebach na terenach poprodukcyjnych. *Przemysł Chem.* **2017**, *96*, 53–57. [[CrossRef](#)]
30. Muyumba, D.K.; Pourret, O.; Liénard, A.; Bonhoure, J.; Mahy, G.; Luhembwe, M.N.; Colinet, G. Mobility of Copper and Cobalt in Metalliferous Ecosystems: Results of a Lysimeter Study in the Lubumbashi Region (Democratic Republic of Congo). *J. Geochem. Explor.* **2019**, *196*, 208–218. [[CrossRef](#)]
31. Bartkiewicz, B. *Oczyszczanie Ścieków Przemysłowych*; Wydawnictwo Naukowe PWN: Warszawa, Poland, 2002.
32. Kabata-Pendias, A.; Pendias, H. *Biogeochemia Pierwiastków Śladowych*; Wydawnictwo Naukowe PWN: Warszawa, Poland, 1999.
33. Komadel, P. Chemically modified smectites. *Clay Miner.* **2003**, *38*, 127–138. [[CrossRef](#)]
34. Bergaya, F.; Theng, B.K.G.; Lagaly, G. Modified clays and clay minerals. In *Handbook of Clay Science*; Bergaya, F., Theng, B.K.G., Lagaly, G., Eds.; Elsevier Science: Amsterdam, The Netherlands, 2006; Volume 1, pp. 261–422.
35. Kunecki, P.; Panek, R.; Wdowin, M.; Franus, W. Synthesis of faujasite (FAU) and tschernichite (LTA) type zeolites as a potential direction of the development of lime Class C fly ash. *Int. J. Miner. Process.* **2017**, *166*, 69–78. [[CrossRef](#)]
36. Espantaleon, A.G.; Nieto, J.A.; Fernandez, M.; Marsal, A. Use of activated clays in the removal of dyes and surfactants from tannery waste waters. *Appl. Clay Sci.* **2003**, *24*, 105–110. [[CrossRef](#)]
37. Jozefaciuk, G.; Bowanko, G. Effect of acid and alkali treatments on surface areas and adsorption energies of selected minerals. *Clays Clay Miner.* **2002**, *50*, 771–783. [[CrossRef](#)]
38. Al-Jlil, S.A. Adsorption of cobalt ions from waste water on activated Saudi clays. *Appl. Water Sci.* **2017**, *7*, 383–391. [[CrossRef](#)]
39. Polish std. PN-ISO 1171:2002P. Paliwa stałe, Oznaczanie popiołu, Wydawnictwa Normalizacyjne, Warszawa. Available online: <http://sklep.pkn.pl/pn-iso-1171-2002p.html> (accessed on 10 October 2002).
40. Choma, J.; Jaroniec, M. Standardowe dane adsorpcji azotu, argonu i benzenu do charakterystyki nanoporowatych adsorbentów krzemionkowych. *Ochr. Środowiska* **2004**, *2*, 3–10.
41. Choma, J.; Zdenkowski, J.A. Standardowe dane adsorpcji azotu do charakterystyki porowatych adsorbentów mineralnych. *Ochr. Środowiska* **2000**, *4*, 3–7.
42. Anvir, D.; Farin, D.; Pfeifer, P. Molecular fractal surfaces. *Nature* **1984**, *308*, 261–263. [[CrossRef](#)]
43. Hofmann, T.; Wallacher, D.; Huber, P.; Birringer, R.; Knorr, K.; Schreiber, A.; Findenegg, G.H. Small-angle X-ray diffraction of Kr in mesoporous silica: Effects of microporosity and surface roughness. *Phys. Rev. B* **2005**, *72*, 064122. [[CrossRef](#)]
44. Wang, F.; Li, S. Determination of the surface fractal dimension for porous media by capillary condensation. *Ind. Eng. Chem. Res.* **1997**, *5*, 1598–1602. [[CrossRef](#)]

45. Lowell, S.; Shields, J.E.; Thomas, M.A.; Thommes, M. *Characterization of Porous Solids and Powders: Surface Area, Pore Size and Density*; Springer Science + Business Media: New York, NY, USA, 2004. [CrossRef]
46. Limousin, G.; Gaudet, J.P.; Charlet, L.; Sznknect, S.; Barthès, V.; Krimissa, M. Sorption isotherms: A review on physical bases, modeling and measurement. *Appl. Geochem.* **2007**, *22*, 249–275. [CrossRef]
47. Cañizares, P.; Valverde, J.L.; Sun Kou, M.R.; Molina, C.B. Synthesis and characterization of PILCs with single and mixed oxide pillars prepared from two different bentonites. A comparative study. *Microporous Mesoporous Mater.* **1999**, *29*, 267–281. [CrossRef]
48. Thommes, M.; Kaneko, K.; Neimark, A.V.; Olivier, J.P.; Rodriguez-Reinoso, F.; Rouquerol, J.; Sing, K.S.W. Physisorption of gases, with special reference to the evaluation of surface area and pore size distribution (IUPAC Technical Report). *Pure Appl. Chem.* **2015**, *87*, 1051–1069. [CrossRef]
49. Sing, K.S.W.; Williams, R.T. Physisorption hysteresis loops and the characterization of nanoporous materials. *Adsorpt. Sci. Technol.* **2004**, *22*, 773–782. [CrossRef]
50. Toor, M.; Jin, B. Adsorption characteristics, isotherm, kinetics, and diffusion of modified natural bentonite for removing diazo dye. *Chem. Eng. J.* **2012**, *187*, 79–88. [CrossRef]
51. Arya, V.; Philip, L. Adsorption of pharmaceuticals in water using Fe₃O₄ coated polymer clay composite. *Microporous Mesoporous Mater.* **2016**, *232*, 273–280. [CrossRef]
52. Bhattacharyya, K.G.; Gupta, S.S. Removal of Cu(II) by natural and acid-activated clays: An insight of adsorption isotherm, kinetic and thermodynamics. *Desalination* **2011**, *272*, 66–75. [CrossRef]
53. Fijał, J.; Kłapyta, Z.; Żabiński, W.; Żyła, M. *Własności Powierzchniowe Mineralów Ilastych i Możliwości Ich Modyfikacji*; Series: Prace Mineralogiczne; Wrocław-Kraków, Zakład Narodowy im. Ossolińskich: Wrocław, Poland, 1980; Volume 65.
54. Bruckman, K.; Fijał, J.; Haber, J.; Kłapyta, Z.; Wiltowski, T.; Żabiński, W. Influence of different activation methods on the catalytic properties of montmorillonite. *Miner. Pol.* **1976**, *7*, 5–14.
55. Belzunce, M.J.; Mendioroz, S.; Haber, J. Modification of sepiolite by treatment with fluorides: Structural and textural changes. *Clays Clay Miner.* **1998**, *46*, 603–614. [CrossRef]
56. Madejová, J.; Bujdák, J.; Janek, M.; Komadel, P. Comparative FT-IR study of structural modifications during acid treatment of dioctahedral smectites and hectorite. *Spectrochim. Acta Part A Mol. Biomol. Spectrosc.* **1998**, *54*, 1397–1406. [CrossRef]
57. Komadel, P.; Madejová, J. Acid activation of clay minerals. In *Handbook of Clay Science*; Bergaya, F., Theng, B.K.G., Lagaly, G., Eds.; Elsevier: Amsterdam, The Netherlands, 2006; pp. 263–288.
58. Rassineux, F.; Griffault, L.; Meunier, A.; Berger, G.; Petit, S.; Vieillard, P.; Zellagui, R.; Munoz, M. Expandability-layer stacking relationship during experimental alteration of a Wyoming bentonite in pH 13.5 solutions at 35 and 60 °C. *Clay Miner.* **2001**, *36*, 197–210. [CrossRef]
59. Melo, J.D.D.; de Carvalho Costa, T.C.; de Medeiros, A.M.; Paskocimas, C.A. Effects of thermal and chemical treatments on physical properties of kaolinite. *Ceram. Int.* **2010**, *36*, 33–38. [CrossRef]
60. Petri, B.G.; Watts, R.J.; Teel, A.L.; Huling, S.G.; Brown, R.A. Fundamentals of ISCO using hydrogen peroxide. In *In Situ Chemical Oxidation for Groundwater Remediation*; Siegrist, R.L., Crimi, M., Simpkin, T.J., Eds.; Springer Science + Business Media: New York, NY, USA, 2011; pp. 33–88. [CrossRef]
61. Ratajczak, T.; Hycnar, E.; Bożęcki, P. The beidellite clays from the Bełchatów lignite deposit as a raw material for constructing waterproofing barriers. *Gospod. Surowcami Miner. Miner. Res. Manag.* **2017**, *33*, 53–68. [CrossRef]
62. Demiral, H.; Güngör, C. Adsorption of copper (II) from aqueous solutions on activated carbon prepared from grape bagasse. *J. Clean. Prod.* **2016**, *124*, 103–113. [CrossRef]
63. Ben-Ali, S.; Jaouali, I.; Souissi-Najar, S.; Ouederni, A. Characterization and adsorption capacity of raw pomegranate peel biosorbent for copper removal. *J. Clean. Prod.* **2017**, *142*, 3809–3821. [CrossRef]
64. Sen Gupta, S.; Bhattacharyya, K.G. Influence of acid activation on adsorption of Ni(II) and Cu(II) on kaolinite and montmorillonite: Kinetic and thermodynamic study. *Chem. Eng. J.* **2008**, *136*, 1–13.
65. Mu'azu, N.D.; Bukhari, A.; Munef, K. Effect of montmorillonite content in natural Saudi Arabian clay on its adsorptive performance for single aqueous uptake of Cu(II) and Ni(II). *J. King Saud Univ. Sci.* **2018**. [CrossRef]
66. Bansal, R.C.; Goyal, M. *Activated Carbon Adsorption*; CRC Press, Taylor & Francis Group: Boca Raton, FL, USA, 2005.

